IEEE Access
Multidisciplinary | Rapid Review | Open Access Journal

Received September 22, 2021, accepted October 14, 2021, date of publication October 21, 2021, date of current version October 26, 2021.

Digital Object Identifier 10.1109/ACCESS.2021.3120991

A Global Decoupling Control Algorithm for LC-DM Adaptive Optics System

YUKUN WANG, XINGYUN ZHANG, DAYU LI, QUANQUAN MU, AND LI XUAN

State Key Laboratory of Applied Optics, Changchun Institute of Optics, Fine Mechanics and Physics, Chinese Academy of Sciences, Changchun 130033, China

Corresponding author: Quanquan Mu (muquanquan@ciomp.ac.cn)

This work was supported in part by the National Natural Science Foundation of China (NSFC) under Grant 12004381, and in part by the State Key Laboratory of Applied Optics, Changchun Institute of Optics, Fine Mechanics and Physics, Chinese Academy of Sciences.

ABSTRACT The liquid crystal (LC) and deformable mirror (DM) cascaded adaptive optics (AO) system can be used to effectively extend the imaging waveband of a large aperture telescope from the infrared to the visible waveband. However, to maintain the effectiveness and stability of the LC-DM AO system, the issues of synchronization and cross-coupling must be resolved. This study proposed a global decoupling control algorithm to simultaneously control the two correctors with high precision. The global decoupling control matrix has been constructed using an eigenmode orthogonal basis and a constraint matrix. The eigenmode orthogonal basis has been derived from the response matrix of the DM and is used for selectively distributing the large stroke low-order aberration to the DM and the remaining aberration to the LC. The constraint matrix has been derived from the projection of the LC response matrix onto the DM eigenmode orthogonal basis, which is used for restraining the LC generating the cross-coupling shape with the DM. The control vectors for both correctors have been calculated simultaneously using the global decoupling control matrix. Numerical simulation indicates that this algorithm exhibits good performance in correcting the different spatial frequency aberrations simultaneously and suppressing the cross-coupling between the dual correctors. Compared to the typical Zernike decomposition algorithm, this algorithm can make full use of the compensation ability of LC-DM. An experiment was conducted on the LC-DM AO system for a 2 m telescope. The experimental results demonstrate that this algorithm is practical for the LC-DM AO system. The cross-coupling between the dual correctors can be restrained well for static and dynamic aberrations simultaneously.

INDEX TERMS Wavefront decoupling, adaptive optics, liquid crystal, deformable mirror.

I. INTRODUCTION

Adaptive optics (AO) is an efficient technology used for compensating wavefront aberration and has been widely used on ground-based large aperture telescopes such as the Very Large Telescope (VLT), Gemini, Keck, Subaru, etc. [1]–[7]. However, almost all large aperture telescopes work in the infrared waveband due to the limitation of the number of actuators of the deformable mirror (DM). Since the shorter the wavelength, the higher is the resolution of the diffraction limit of the telescope, and since the high-sensitivity imaging camera is also the most effective in the visible waveband, the realization of an AO system for the visible waveband will offer additional information in the field of astronomical and space target observations. Hence, an AO system is required for simultaneously compensating a large stroke and high spatial frequency aberration in the visible waveband. For a single DM, a large stroke and high spatial frequency cannot be achieved at the same time owing to the limitation imposed by its fabrication technology [8]. Thus, a woofer-tweeter (W-T) AO system with two DMs is an effective means of achieving this goal [9], [10]. The most famous is the PALM-3000 AO system on the 5.1 m Hale Telescope [11], which contains two DMs with 241 and 3388 actuators, respectively. Although this AO system can compensate for the aberrations in the visible waveband, it is very expensive and difficult to realize [12]. Furthermore, an aperture that is greater than 5.1 m cannot work in the visible waveband since there has been no follow-up application report on the number of actuators of the DM larger than 3388 that are in the PALM-3000 AO system.

The associate editor coordinating the review of this manuscript and approving it for publication was Yong Yang.

This work is licensed under a Creative Commons Attribution 4.0 License. For more information, see https://creativecommons.org/licenses/by/4.0/

In contrast to the dual DM AO system, a liquid crystal (LC) wavefront corrector has been used as the tweeter to construct an LC and DM cascaded AO system [13]. The LC has the advantages of high spatial frequency, easy fabrication, and low cost but has the shortcomings of narrow working waveband in the visible waveband due to its slow response in the infrared waveband and dispersion. The DM has the advantages of a wide working waveband and fast response but has the shortcomings of low spatial frequency, the difficulty of fabrication, and high cost. The advantages and disadvantages of the LC and DM are complementary. Hence, LC is suitable for compensating the small stroke high spatial frequency aberration in the visible waveband. In contrast, the large stroke low spatial frequency aberration in the full waveband can be compensated by the DM. This is an effective solution for extending the imaging waveband of large aperture telescopes to the visible waveband.

As the aberrations corrected by the W-T AO system are measured by single WFS, the control algorithms are critical for distributing the aberrations and suppressing the cross-coupling between the two correctors. Otherwise, the cross-coupling will result in the waste of the correctors' stroke and even make the system unstable. The aberration can be compensated step by step or synchronously. Many control algorithms for the dual-DM AO system have been proposed. When the correctors are controlled step by step, which is called dual step control algorithm [14], it is a time sequencing problem. The aberration from WFS is compensated by a low-order corrector, and then the residual aberration is detected and compensated by a high-order corrector. Since the aberrations for the correctors are detected step by step, it can avoid the accumulation of the cross-coupling errors. However, the correction procedure is time consuming, thus it cannot be used for the cases where the wave front aberrations vary rapidly. It can only be applied to a static aberration correction. When the two correctors work at the same time and compensate the aberrations detected from single WFS at the same time, there is cross-coupling problem. The cross-coupling problem is caused by the different spatial distribution characteristics of the two correctors and the wave front detection scheme of the single WFS, the simultaneous control of the two correctors without coupling is a global decoupling control problem, the problem of wave front decomposition and decoupling should be solved, so that the good quality image can be achieved both in infrared waveband and in the visible waveband at the same time. There are several global control algorithms such as the zonal control algorithm [15], and the modal control algorithm [16]. For the zonal control algorithm, such as the Lagrange-multiplier damped least-squares algorithm [17], the cross-coupling error, accumulated during a long-time correction, cannot be described accurately. Among the different methods such as the Zernike mode [18], Fourier mode [19], Wavelet mode [20], etc., the Zernike mode is the most common and useful method for modal control owing to its correspondence with the wavefront aberration. The wavefront can be reconstructed and distributed to the two correctors, and a constraint matrix with the Zernike mode will reset the commands of the tweeter. In addition, cross-coupling can be suppressed efficiently by this method as compared to the suppression achieved by the zonal control algorithm.

Based on the research on the dual-DM control algorithm, the dual step and Zernike mode control algorithm have been introduced into the LC-DM AO system. A good static aberration correction was achieved [21], but it did not realize dynamic wave front correction. This is due to the different characteristics of LC-DM and dual DMs. Firstly, the working mode of the LC is open-loop to improve its energy utilization [22], as is shown in Fig. 1. The LC corrector has its problems such as wavelength dependence, dispersion and working under polarized light. Hence, the energy utilization is lower in LC close loop AO system than LC open loop AO system. In the close loop, S-polarized light must be divided into part of the light to enter the WFS for the residuals detection. The open-loop system directly uses P-polarized light to enter the WFS, and all the S-polarized light is used for imaging. Our team's research in the field of open loop LC AO system started in 2000. The relevant conclusions on open loop LC AO systems have been verified in reference [22] and engineering application [27]. The aberration after LC correction cannot be detected, and the cross-coupling cannot be calculated from the WFS. Secondly, the number of pixels of an LC is massive and cannot be driven individually, as is done in a DM. Hence, the LC is usually driven by shape according to the Zernike mode. However, the slope response of the Zernike modes measured by the WFS is not orthogonal. Thirdly, the construction of the constraint matrix requires an accurate influence function of the LC and the DM. The process of Zernike mode reconstruction and cross-coupling suppression is time-consuming. Finally, the DM cannot fit all the Zernike modes accurately, and the correction ability of the DM is not fully used.

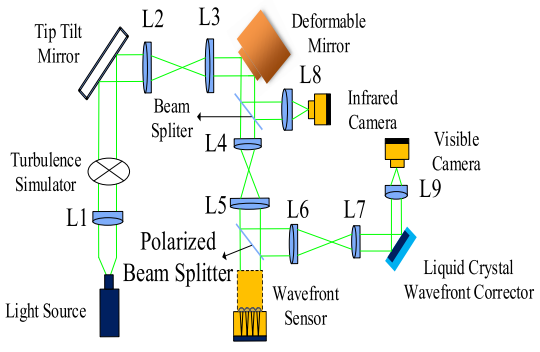

FIGURE 1. Schematic of the LC-DM AO system.

This study proposes a global decoupling control algorithm that can simultaneously obtain the command vectors for each corrector and suppress the cross-coupling errors. The global control matrix is composed of an eigenmode orthogonal basis and a constraint matrix. The eigenmode orthogonal basis has

been derived from the response matrix of the DM measured by WFS, which can make full use of the correction ability of the DM and improve the correction accuracy of the DM [23]. Further, the eigenmode orthogonal basis has been used for distributing the wave front aberration according to the imaging requirements of the diffraction limit in the infrared waveband. The residual aberration after DM correction has been used for calculating the LC driving command to meet the requirement of the diffraction limit in the visible waveband. The constraint matrix has been derived from the projection of the LC response matrix onto the DM eigenmode orthogonal basis and used for removing the cross-coupling between the LC and the DM. This algorithm is effective and computationally simple, with the slope signal measured by the WFS. The numerical simulation and the experimental results show that this algorithm is valid and practical for the LC-DM AO system. Compared to the traditional Zernike decomposition algorithm, the algorithm proposed in this work can realize dynamic wavefront correction.

II. PRINCIPLE OF THE GLOBAL DECOUPLING CONTROL ALGORITHM

A. DERIVATION OF THE EIGENMODE ORTHOGONAL BASIS

In the LC-DM AO system, the response matrix of the LC R_{LC} $(2n \times m_{LC})$ and the DM R_{DM} $(2n \times m_{DM})$ are measured by a Shark-Hartmann WFS (S-H WFS), where n is the number of valid sub apertures, m_{LC} is the number of Zernike modes for the LC correction, m_{DM} is the number of DM actuators. The slope $g(2n \times 1)$ of the wavefront aberration is compensated by the LC and DM, and can be written as:

$$g = R_{LC} v_{LC} + R_{DM} v_{DM} \tag{1}$$

where $v_{LC}(m_{LC} \times 1)$ are the Zernike coefficients that drive the LC. $v_{DM}(m_{DM} \times 1)$ is the voltage vector for driving the DM. Next, a reasonable distribution of the aberrations is indispensable. Since, the slope response matrix of the DM is non-orthogonal, various modal decomposition algorithms, such as the Zernike modes [18], have been proposed for reconstructing the slope to the modes. However, this process is time-consuming and can introduce reconstruction error. In addition, the selection of the mode number and the fitting ability of the DM for different modes also influence its correction performance. Thus we directly distribute the aberration based on the slope response matrix of the DM, which not only avoids the process of reconstruction, but also makes full use of the correction ability of the DM. To achieve this goal, the coupling matrix C $(m_{DM} \times m_{DM})$ between the actuators is calculated as:

$$C(i, j) = C(j, i) = D^{-1} \int_D R_{DM(i)} R_{DM(j)} dxdy \tag{2}$$

where D is the aperture of the DM. Then, the singular value decomposition of the coupling matrix is performed using,

$$C = USU^T \tag{3}$$

where S $(m_{DM} \times m_{DM})$ is a diagonal matrix composed of the singular value of the matrix C, and U $(m_{DM} \times m_{DM})$ is a unitary matrix formed by the eigenvector of the matrix C. The eigenmode of the DM is the linear combination of the unitary matrix U and the response matrix R_{DM}:

$$M_i = \sum_{j=1}^{m_{DM}} U(i, j) R_{DM(j)}, \quad i = 1, 2, \cdots, m_{DM} \tag{4}$$

where M_i $(2n \times 1)$ is the i-th eigenmode. The slope response g_{DM} $(2n \times 1)$ of the DM can be described as:

$$g_{DM} = M \cdot m \tag{5}$$

where $m(m_{DM} \times 1)$ is the eigenmode coefficient, $M = \left[M_1, M_2, \cdots, M_{m_{DM}}\right]$ is the eigenmode response matrix of the DM, which is mutually orthogonal, and the spatial frequency of the DM eigenmodes are arranged from low to high according to the modes. Theoretically, the DM can fit all the eigenmodes well. In order to improve the accuracy of the correction, we use the eigenmode coefficient to represent the DM response matrix,

$$R_{DM(i)} = M \cdot m_{R_{DM(i)}} \tag{6}$$

where $m_{R_{DM(i)}}(m_{DM} \times 1)$ is the eigenmode coefficient vector corresponding to the response of the i-th actuator. Hence, Equation(5) can be rewritten as

$$g_{DM} = R_{DM} \cdot v_{DM} \approx M_R \cdot v_{DM} = M \cdot m_{R_{DM}} \cdot v_{DM} \tag{7}$$

where $m_{R_{DM}} = \left[m_{R_{DM(1)}}, m_{R_{DM(2)}}, \cdots, m_{R_{DM(m_{DM})}}\right]$ can be calculated with $m_{R_{DM}} = M^+ R_{DM}$ and M^+ is the pseudo-inverse matrix of M. $M_R = M \cdot m_{R_{DM}}$ is defined as the eigenmode orthogonal basis. Then, we can selectively distribute the aberration for the DM with a diagonal matrix $I_N(m_{DM} \times m_{DM})$,

$$g_{DM} = R_{DM} \cdot (M \cdot I_N \cdot m_{R_{DM}})^+ \cdot g \tag{8}$$

$$\mathrm{I_N} = \begin{bmatrix} 1 & & & & 0 \\ & \ddots & & & \\ & & 1 & & \\ & & & 0 & \\ & & & & \ddots \\ 0 & & & & 0 \end{bmatrix} \tag{9}$$

where the selected diagonal elements are one whereas others are zero.

B. DECOUPLING BETWEEN THE LC AND THE DM

The residual wave front aberrations g_{LC} $(2n \times 1)$ will be compensated by the LC and can be solved using Equation (10).

$$g_{LC} = g - (M \cdot I_N \cdot m_{R_{DM}})^+ \cdot g = (I - (M \cdot I_N \cdot m_{R_{DM}})^+) \cdot g \tag{10}$$

where I is the $2n \times 2n$ identity matrix. In order to prevent the LC from generating the aberrations that have been compensated by the DM, we need to build a new set of response matrix R'_{LC}, from the measured response matrix R_{LC}.

R'_{LC} is orthogonal to the selected eigenmode orthogonal basis M_R. The minimum variance fit of R_{LC} on M_R can be obtained by minimizing the Frobenius norm

$$J_F = \|R_{LC} - M_R \cdot P\|^2 \tag{11}$$

where $P(m_{DM} \times m_{LC})$ is the constraint matrix that represents the projection matrix of R_{LC} onto $I_N \cdot M_R$. It can be obtained by solving the following equation:

$$\begin{aligned}\frac{\partial J_F}{\partial P} &= \frac{\partial}{\partial P} trace\left(R_{LC}R_{LC}^T - I_N R_{LC} P^T M_R^T \right.\\ &\quad \left. - I_N M_R P F^T + I_N M_R P P^T M_R^T\right)\\ &= -2I_N M_R^T R_{LC} + 2I_N M_R^T M_R P = 0\end{aligned} \tag{12}$$

Then,

$$P = (M \cdot I_N \cdot m_{R_{DM}})^+ \cdot R_{LC} \tag{13}$$

The matrix P represents the expansion coefficients of R_{LC} in the $I_N \cdot M_R$ space, and the new decoupling response matrix, R'_{LC}, can be obtained as follows:

$$R'_{LC} = R_{LC} - M_R \cdot (M \cdot I_N \cdot m_{R_{DM}})^+ \cdot R_{LC} \tag{14}$$

The correction of g_{LC} can be described as

$$g_{LC} = R'_{LC} \cdot v_{LC} \tag{15}$$

C. CONSTRUCTION OF THE GLOBAL DECOUPLING CONTROL MATRIX

From Equations (7) and (8), the control command, $C_{DM}(m_{DM} \times 2n)$, of the DM can be expressed as

$$v_{DM} = M_R^+ \cdot R_{DM} \cdot (M \cdot I_N \cdot m_{R_{DM}})^+ \cdot g = C_{DM} \cdot g \tag{16}$$

whereas from Equations (10) and (15), the control command, $C_{LC}(m_{LC} \times 2n)$ of the LC can be expressed as

$$v_{LC} = R_{LC}^{'+} \cdot (I - (M \cdot I_N \cdot m_{R_{DM}})^+) \cdot g = C_{LC} \cdot g \tag{17}$$

Finally, we can calculate the command vector, V ($(m_{DM} + m_{LC}) \times 1$), for the LC and DM using the global decoupling control matrix, $C_{global}(m_{DM} + m_{LC}) \times 2n$, simultaneously via

$$V = \begin{bmatrix} v_{DM} \\ v_{LC} \end{bmatrix} = C_{global} \cdot g = \begin{bmatrix} C_{DM} \\ C_{LC} \end{bmatrix} \cdot g \tag{18}$$

The DM works under the closed-loop mode, and its driving voltage, V_{DM}, is calculated by a digital proportional integral derivative (PID) controller according to Equation (19) [13]. The LC works under the open-loop mode, and its driving voltage, V_{LC}, is calculated using the Proportional-Derivative (PD) controller according to Equation (20) [25]. PD controller is widely used in closed loop systems for its effectiveness, simplicity and robust. The proportional element is used to guarantee the system performance in low frequency, and a derivative element is used to improve the system performance in high frequency. In fact, the derivative element is a D-step prediction of the aberration, so the parameter D is determined by the total time delay of the system. More information can be found in reference [25].

$$\begin{aligned}V_{DM}(k+1) &= V_{DM}(k) + K_P(v_{DM}(k) - v_{DM}(k-1))\\ &\quad + K_I v_{DM}(k) + K_D(v_{DM}(k) - 2v_{DM}(k-1)\\ &\quad + v_{DM}(k-2))\end{aligned} \tag{19}$$

$$V_{LC}(k+1) = K'_P v_{LC}(k) + K'_D(v_{LC}(k) - v_{LC}(k-1)) \tag{20}$$

where K_P, K_I, K_D, K'_P, and K'_D are the parameters of the controller. The system bandwidth is a crucial requirement for an AO system. It directly limits the turbulence coping capability of the system. A larger bandwidth leads to lower residual aberrations. The best bandwidth can be obtained by adjusting the parameters of the controller. A bad tuning of these parameters decreases the bandwidth of the control system and leads to poor correction performance. The tuning law and experimental results are given in reference [13], [25] and [26].

III. NUMERICAL SIMULATION

A. SIMULATION MODEL

In order to verify the above algorithm, a simulation model of the LC-DM AO system was built. In the simulation model, the number of actuators of the DM was 145, the pitch of the DM was 2.5 mm, and its aperture was 30 mm. The density of the LC was 256 × 256 pixels, and the aperture was 6.1 mm. The number of sub-apertures of the WFS was 20 × 20, and the full aperture was 5.8 mm. These devices were conjugated and scaled using a 4f optical system to enable identical measurement and correction of the wave front. The influence function, W_{DM}, of the DM was described as a Gaussian function, as given in Equation (21). The LC was described with a 209 Zernike mode polynomial.

$$W_{DM(i)} = \exp\left[\ln\omega\left(\sqrt{(x - x_i)^2 + (y - y_i)^2}/d\right)^{\alpha}\right] \tag{21}$$

where α, ω and d are the Gaussian exponent, the coupling value, and the spacing between the actuators in the DM, respectively. In this model, α was 1.73, ω was 0.23, and d was set to 0.083. These parameters are taken from the DM that was purchased from ALPAO. The configuration of the actuators of the DM and the surface of the LC with the sub-apertures of the WFS are shown in Fig. 2. The black spots are the actuators of the DM, the intensive red spots represent the pixels of the LC, and the blue grid is the sub-apertures of the WFS. The black circle is the valid aperture of the wave front.

Depending on the configuration of Fig. 2, the slope response matrix of the LC, $R_{LC}(800 \times 209)$, and the DM, R_{DM} (800×145), can be calculated. The partial slope values of R_{LC} and R_{DM} are plotted in Fig. 3.

Using the slope response matrices, the eigenmode orthogonal basis can be calculated using Equations (2)–(4), and the shape of the eigenmode thus obtained is shown in Fig. 4.

From Fig. 4, it can be seen that the spatial frequency of the eigenmode increases with the order and can be used for

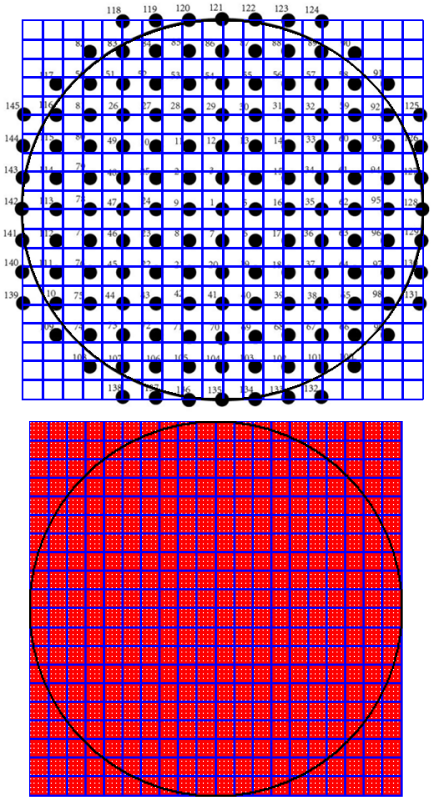

FIGURE 2. Configuration of the actuators of the DM and the surface of the LC with the sub-apertures of the WFS. The up part shows the DM, whereas the down part shows the LC.

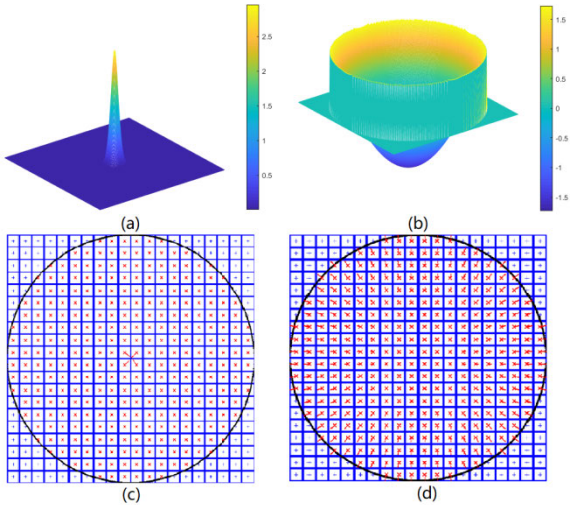

FIGURE 3. The surface and the slope response of the DM and the LC. (a),(c) show the 1st actuator of the DM, whereas (b),(d) show the 3rd Zernike mode of the LC.

allocating the aberration to the two correctors. The correlation of the column vector of M_R is shown in Fig. 5.

From Fig. 5, it can be seen that the column of M_R is completely orthogonal. Then, the constraint matrix, P, can be calculated as shown in Fig. 6.

With the constraint matrix and the eigenmode orthogonal basis, we can selectively distribute the large-amplitude

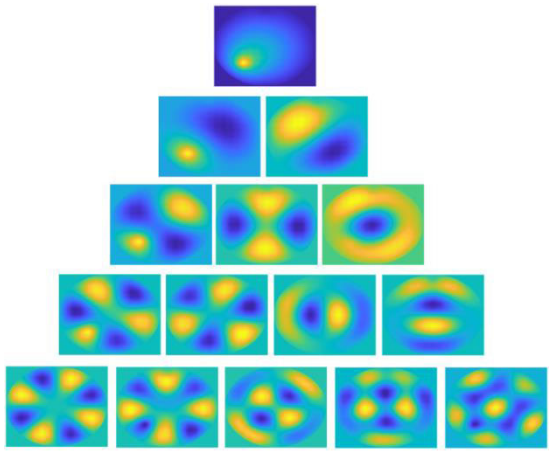

FIGURE 4. Shape of the eigenmode M in the top 15 column vectors.

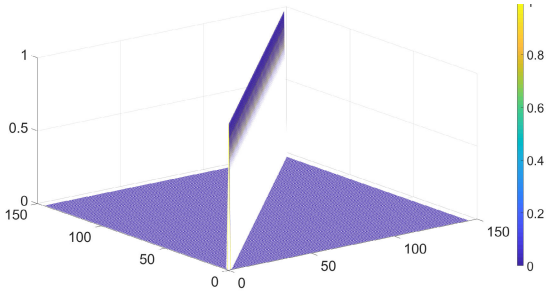

FIGURE 5. Correction of the column vector of M_R.

low-order aberration to the DM and the remaining aberration to the LC. Finally, the global decoupling control matrix is constructed using Equations (16)–(18).

B. CORRECTION PERFORMANCE

After establishing the simulation model, An atmospheric turbulence was generated to verify the compensation ability of our algorithm. In the simulation, the atmospheric turbulence was of medium intensity, the telescope diameter, D, was 2 m, and the atmosphere coherence length r0 was 10 cm @ 785 nm. Figure 7 shows the top 209 Zernike coefficients and the shape of the initial aberration. The peak-to-valley (PV) and the root mean square (RMS) values of the initial aberrations were 8.91 μm and 1.51 μm, respectively.

Generally, when the Strehl Ratio (SR) reaches 0.8 in an optical system, the high-contrast diffraction-limited resolution imaging can be achieved. According to this criterion, the Strehl Ratio at the center wavelength of each imaging waveband should reach 0.8 after AO correction. According to the relationship between SR and wavefront residual σ:

$$\mathrm{SR} = \mathrm{e}^{-(k\sigma)^2} \tag{22}$$

$$\sigma = 0.075\lambda \tag{23}$$

where k=$2\pi/\lambda$ is the wave number. For a telescope with an aperture of D=2 meters, r0=10cm @ λ =550nm of moderate turbulence, its r0=25.5cm at λ =1200 nm, 55 eigenmodes

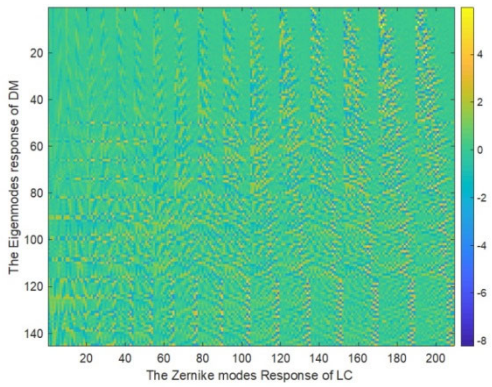

FIGURE 6. The constraint matrix of the response of the LC projected onto the eigenmode response of the DM.

are corrected, the wave front residual is 0.073λ. The same D=2m, r0=19.3cm at λ =950nm, the DM corrects 74 eigenmodes to make this waveband reach the diffraction limit. In the LC-DM cascade AO, the LC is responsible for correcting the 700-950 nm waveband, and the DM is responsible for correcting the 700-1700 nm waveband. As long as the wave front residual is less than 0.075 λ, both wavebands can attain the diffraction limit resolution. According to the eigenmode number and wave front residual formula given in the reference [23], the DM only corrects the top 55 eigenmodes to make the infrared waveband reach the diffraction limit, and the LC performs secondary correction on the residual wave front after the DM correction. After calculation, the LC must correct the top 69 Zernike modes to reach 0.073 λ [24]. Further, a comparison between the global decoupling algorithm proposed in this work and

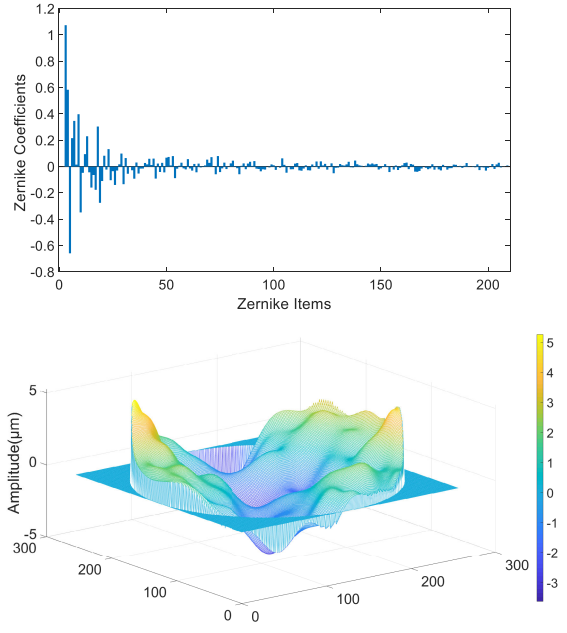

FIGURE 7. The initial aberration for the simulation: (up) Zernike coefficients and (down) shape of the aberration.

the traditional Zernike algorithms was made by adding the same initial aberrations. In the Zernike algorithm, the top 29 Zernike modes were selected for the DM, and the rest of the modes were selected for the LC [21]. The global un-decoupling algorithm was also compared with our algorithm, which replaces the decoupling response matrix, R'_{LC}, in the global decoupling algorithm with the original response matrix, R_{LC}. For the tuning of the DM controller parameters, the Ziegler-Nichols law is used to obtain the initial PID parameters [26], then the K_P is tuned to shorten the response time of the DM, then the K_I is tuned to quickly reduce the residuals without oscillation, and finally the K_D is tuned to keep a small overshoot during the correction [13]. For the tuning of the LC controller parameters, the K'p is tuned to guarantee the system performance at a low frequency, and the K'_D is tuned to improve the system performance at a high frequency. The K'_P is usually a value near 1 in the open loop system and the K'_D is a one-step prediction of the aberration, so the parameter K'_D is determined by the total time delay of the open loop system. According to the experimental results of earlier studies [13] and [25], the control parameters used in Equations (19) and (20) were selected to be K_P =0.9, K_I =0.1, K_D =0.01, and K'_P =0.75, K'_D =2 [13], [25]. The correction results are shown in Fig. 8. To achieve cross-coupling, the coupling coefficient, c, was defined as follows:

$$c = \frac{\left|\iint W_{DM} W_{LC} dD\right|}{\sqrt{\iint W_{DM} W_{DM} dD}\sqrt{\iint W_{LC} W_{LC} dD}} \tag{24}$$

where W_{DM} is the correction of the DM, W_{LC} is the correction of the LC, and D is the aperture of the wave front.

The results of Zernike coefficients of the residual aberration after AO correction with different algorithms are given in Fig. 8. It is obvious that our algorithm enables the dual correctors to correct different spatial frequency aberrations and achieve better compensation results than the global un-decoupling control algorithm and the Zernike control algorithm. Fig. 9 is the residual aberration after low order correction by the DM, where the LC corrector is not involved. As shown in Figs. 9(a)–(c), most of the initial aberration is corrected by the DM. Compared to the traditional Zernike control algorithm, the global control algorithm can achieve better precision than the Zernike mode, as is observed from Figs. 9(a)–(c). The PV and RMS values are 1.71 μm and 0.09 μm after eigenmode correction in Fig 9 (a) and (b). The data shown in Fig. 9 (a) and (b) are the same due to the DM correction in global decoupling and un-decoupling algorithms are done using eigenmodes. The results of DM correction using Zernike modes are shown in Fig.9 (c), the PV and RMS values are 2.78 μm and 0.13 μm after Zernike correction. Hence, we can conclude that the eigenmodes have a better correction performance than the Zernike modes for DM correction. Then, the residual aberration after DM correction is a high spatial frequency and low stroke aberration, which is compensated well by the LC, as observed from Figs. 10(a)–(c). It is worth noting

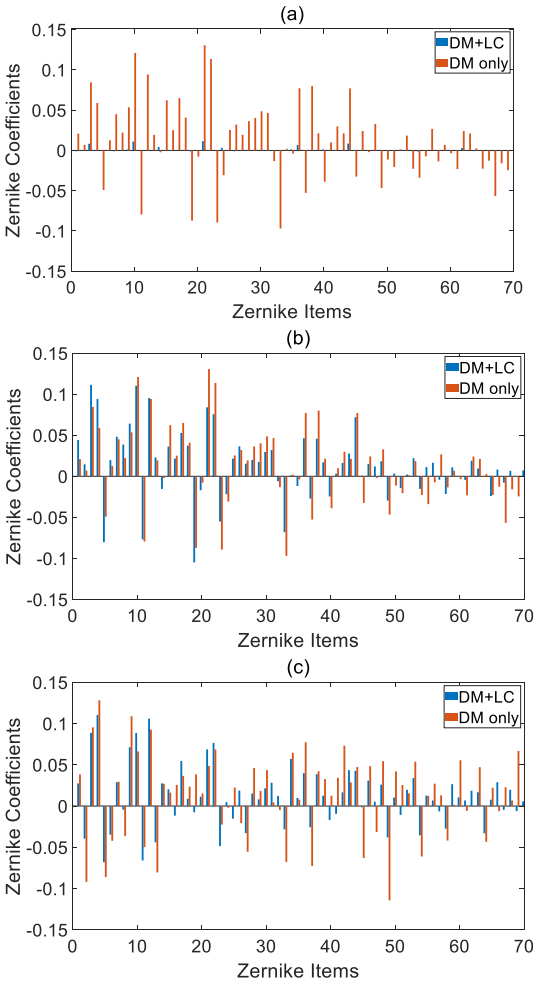

FIGURE 8. Zernike coefficients of the residual aberration after AO correction with different algorithms. (a) show the Global Decoupling algorithm, (b) show the Global Un-decoupling Algorithm and (c) show the Zernike Decoupling Algorithm.

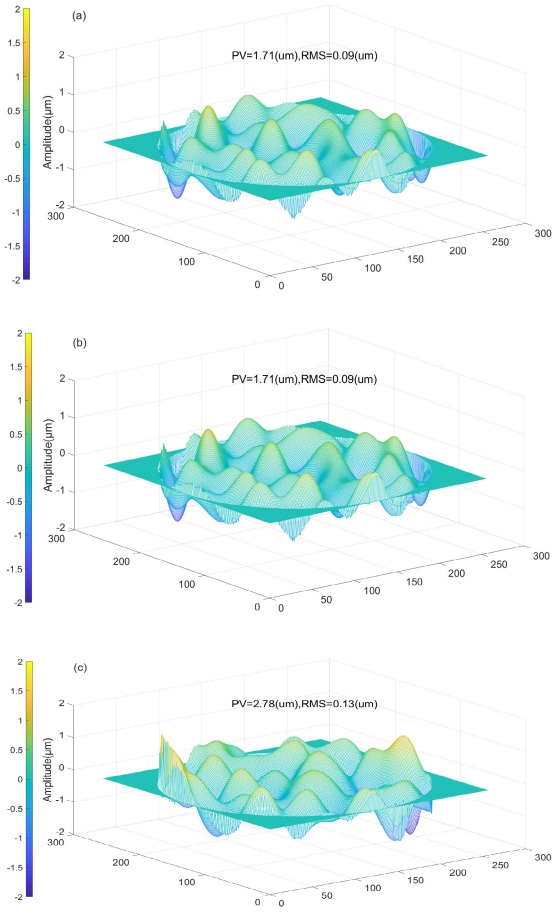

FIGURE 9. Shape of the residual aberration after DM correction with different algorithms. (a) show the Global Decoupling algorithm, (b) show the Global Un-decoupling Algorithm and (c) show the Zernike Decoupling Algorithm.

that the coupling coefficients of the three algorithms are 0.0026, 0.1893, and 0.0108, respectively. The cross-coupling error is eliminated in Fig. 10 (a) but not in Fig. 10 (b). The PV and RMS values obtained using our algorithm are 0.38 μm, and 0.03 μm (Fig. 10(a)), those obtained using the global un-decoupling algorithm are 0.88 μm and 0.06 μm (Fig. 10(b)), and those obtained using the Zernike decoupling algorithm are 1.22 μm and 0.09 μm (Fig. 10(c)), which can be seen that the global decoupling algorithm has a better performance than that of global un-decoupling algorithm and Zernike decoupling algorithm for LC-DM correction. Further, it can be easily concluded that the global decoupling algorithm can simultaneously control the two correctors for different spatial frequency aberration compensation with the least cross-coupling.

IV. EXPERIMENT

A. EXPERIMENTAL SETUP

An experimental DM-LC AO system for the 2 m telescope was established to evaluate the validity of the proposed method. In the optical system, a fiber-coupled Xenon lamp was selected as the light source with a spectrum range of 0.4-1.7 μm. The tip-tilt mirror (TTM) had a 25 mm aperture, $\pm$2 mrad magnitude, and a resonant frequency of 2.6 kHz. The DM was purchased from ALPAO with 145 actuators, 30 mm aperture, and 3 μm stroke. The LC was custom-made by BNS using our liquid crystal material. The aperture of the LC was 6.14 mm and consisted of 256 $\times$ 256 pixels. We designed the S-H WFS for a 2 m telescope and moderate turbulence of r0=10cm @ λ =550nm, the number of sub-apertures was calculated by (D/ r0)^2. Therefore, the S-H WFS used in the experiment was custom-made with a frame rate of 1.67 kHz and 20 $\times$ 20 micro lenses. It is enough for aberration detection at 0.7 - 1.7 μm waveband. An atmospheric turbulence simulator was used for generating the aberration and r0=1 mm at the wavelength of 785 nm. To simulate the atmospheric turbulence for a 2 m telescope with r0=10 cm, the sub-aperture of 20 mm was selected on the phase screen of the atmospheric turbulence.

Based on the selected devices, the optical layout is illustrated in Fig. 11. The light emitted from the fiber is collimated by an achromatic lens, L1, having an aperture of 20 mm and

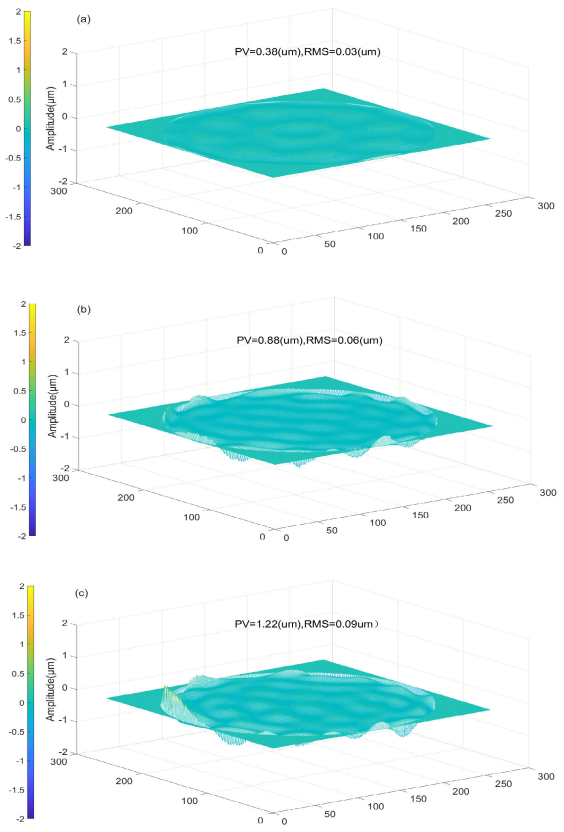

FIGURE 10. Shape of the residual aberration after LC-DM correction with different algorithms. (a) show the Global Decoupling algorithm, (b) show the Global Un-decoupling Algorithm and (c) show the Zernike Decoupling Algorithm.

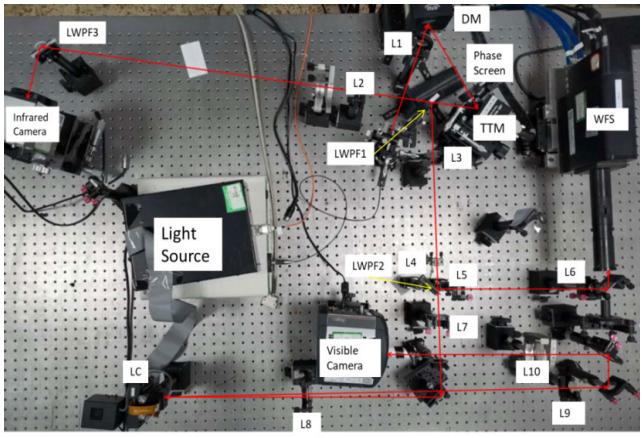

FIGURE 11. Optical layout of the LC-DM AO system.

then reflected by the DM. The reflected beam goes through the phase screen of atmospheric turbulence and is reflected by the TTM. The reflected light is split into two beams by the long wave pass filter 1 (LWPF1) with a split point of 0.95 μm: one is transmitted and focused on the infrared camera through L2, whereas the reflected light is zoomed out with a pair of lenses (L3 and L4) following, which it goes to LWPF2 with a split point of 0.7 μm. The incident light is split by LWPF2 into two beams: one is reflected and enters the S-H WFS through L5 and L6 for aberration detection, whereas the transmitted light is zoomed by L7 and L8 and goes to the LC from, which it is reflected. The reflected light is zoomed by L8 and L9 and finally imaged by a visible CCD camera using L10. Furthermore, the infrared waveband 0.95-1.7 μm is split into 0.95-1.5 μm and 1.5-1.7 μm respectively with LWPF3. In this optical design, the waveband of 0.4–0.7 μm is used for wavefront detection, and the imaging wavebands are 0.7-0.95 μm, 0.95-1.5 μm, and 1.5-1.7 μm respectively. The parameters of the lenses are given in Table 1.

B. THE EIGENMODE CORRECTION OF THE DM IN THE INFRARED BAND

To test the advantage of the eigenmode for the DM correction, a static initial aberration from the phase screen was corrected using the eigenmode and Zernike mode, respectively. In the analysis of the simulation data, the top 55 eigenmodes and the top 29 Zernike modes were selected for the DM to reach the diffraction-limited resolution in the infrared band. The aberration measured before correction resulted in PV=7.152 μm and RMS=0.686 μm (Fig. 12(a)). The residual aberration measured after eigenmode correction resulted in PV = 1.522 μm and RMS=0.097 μm (Fig. 12(b)), and the residual aberration measured after Zernike mode correction resulted in PV=2.191 μm and RMS=0.121 μm (Fig. 12(c)). As the LC works in the open-loop mode, the S-H WFS can only measure the correction error of the DM. Therefore, the results shown in Fig. 12 represent the effectiveness in correction achieved by applying the eigenmode to obtain better precision than the Zernike modes. Using the expression given by Jin *et al.* [23] for the relationship between the residual error and the number of eigenmodes, after the DM corrects 55 eigenmodes, the residual RMS can be reduced to approximately 0.47 rad, which is 0.089 μm at 1200 nm waveband. Thus, the experimental result is consistent with the theoretical result.

TABLE 1. Parameters of Each Lens in the LC-DM AO System

Lens	Focus Length(mm)	Aperture(mm)
L1	200	20
L2	548	20
L3	300	20
L4	-43.5	2.9
L5	100	2.9
L6	200	5.8
L7	150	2.9
L8	300	5.8
L9	300	5.8
L10	272	5.8

To verify the resolution of the system, USAF 1951 target was chosen as the resolution target. The images of the USAF target are shown in Fig. 13 in the waveband of 1.5–1.7 μm

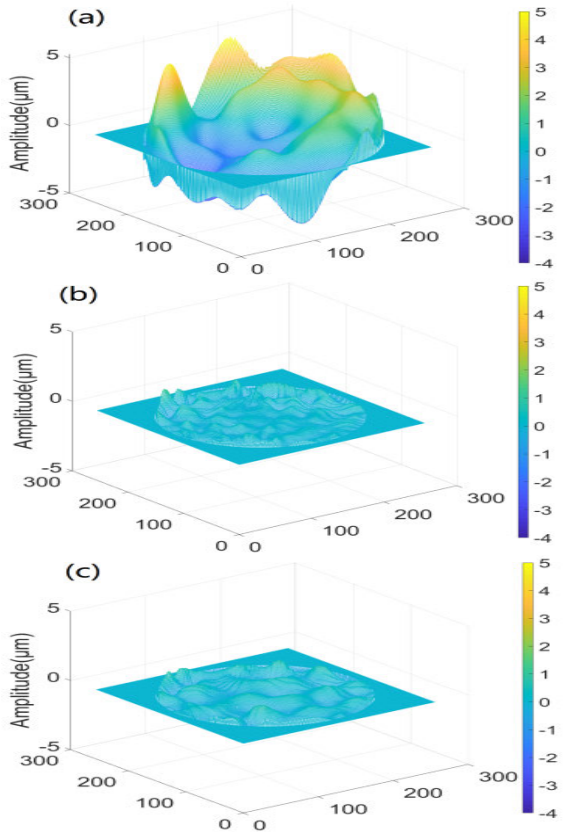

FIGURE 12. Wavefront correction with the DM. (a) Initial aberration, (b) eigenmode correction, (c) Zernike mode correction.

without and with AO correction. The fifth element of the fifth group of the USAF target was resolved after AO correction using each algorithm, which indicates that the resolution capacity of the system is 19.7 μm (50.8 cycles/mm). Considering the entrance pupil of the AO system to be 20 mm, the diffraction-limited resolution was 19.5 μm at 1.6 μm wavelength. Therefore, it can be said that the diffraction-limited resolution was acquired in the waveband of 1.5–1.7 μm after DM correction.

Similarly, the correction results corresponding to the 0.95–1.5 μm waveband were obtained. As can be seen from Fig. 14(b), the first element of the sixth group was resolved after eigenmode correction, and the resolution capacity achieved is 15.6 μm (64 cycles/mm), which is close to the diffraction-limited resolution of 14.6 μm at the wavelength of 1.2 μm. As can be observed from Fig. 14(c), the sixth element of the fifth group was resolved after Zernike mode correction, and the resolution capacity achieved is 17.5 μm (57 cycles/mm), which is 1.2 times the diffraction-limited resolution at the wavelength of 1.2 μm. The results prove that the eigenmode correction method proposed in this study has a higher correction precision than the traditional Zernike mode.

C. CASCADE DECOUPLING CORRECTION OF THE LC-DM IN THE FULL BAND

After DM correction, the residual aberration is sent to the LC. As the LC works in the open-loop mode, the aberration

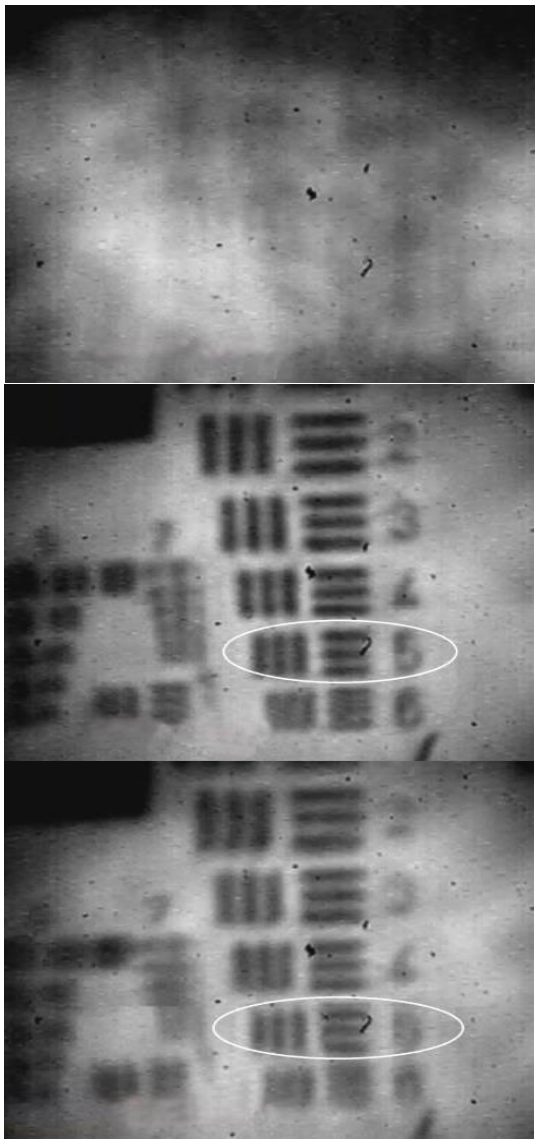

FIGURE 13. Images of the USAF target in the 1.5–1.7 μm waveband (up) without correction, (middle) with eigenmode correction, and (down) with Zernike mode correction.

after LC correction cannot be measured. To verify the effectiveness of cross-coupling suppression, a comparison between the global decoupling algorithm and the global un-decoupling was performed. The images of the USAF target without and with different AO correction algorithms are shown in Fig. 15 in the 0.7-0.95 μm waveband. Fig. 15(b) presents the result with only DM correction, which shows that the image quality of the USAF target is improved, but the elements cannot be resolved clearly. As shown in Fig. 15(c), the fourth element of the sixth group of the target is resolved after the global un-decoupling correction, and the resolution capacity is 11.04 μm (90.5 cycles/mm). As the diffraction-limited resolution is 9.76 μm at the wavelength of 0.8 μm, a resolution greater by a factor of 1.1 is achieved. As seen from Fig. 15(d), the fifth element of the sixth group is resolved after the global decoupling correction,

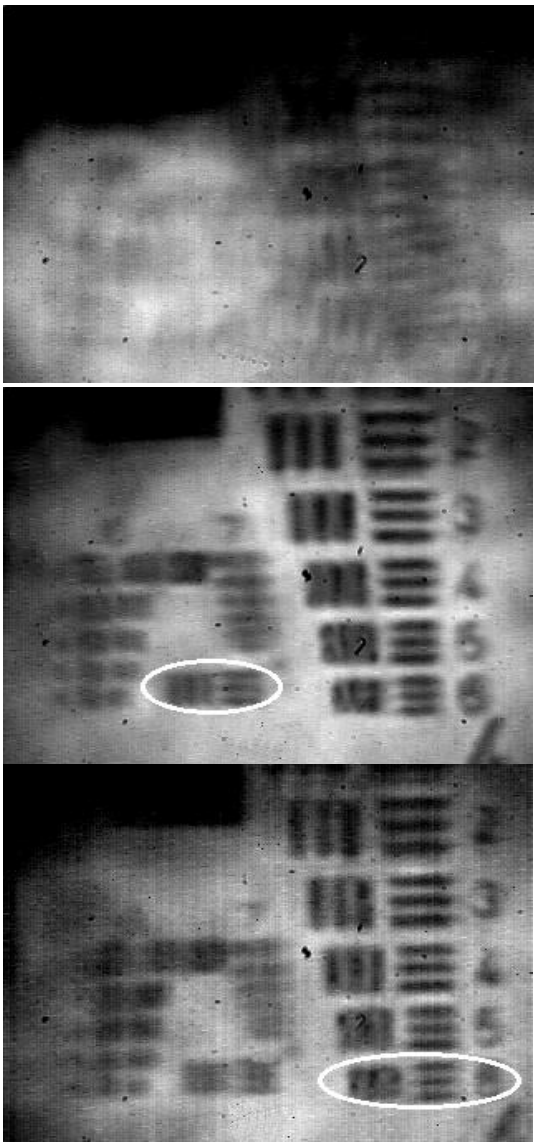

FIGURE 14. Images of the USAF target in the 0.95-1.5 μm waveband (up) without correction, (middle) with eigenmode correction, and (down) with Zernike mode correction.

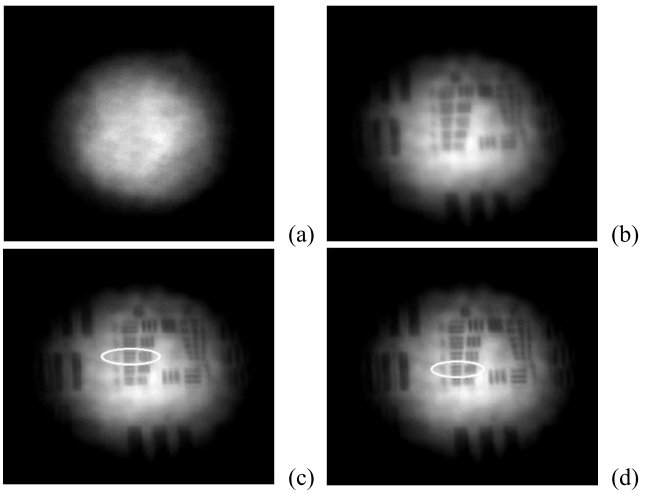

FIGURE 15. Images of the USAF target in the 0.7–0.95 μm waveband (a) without correction, (b) with eigenmode correction of the DM, (c) with the global un-decoupling correction of the LC-DM, and (d) with the global decoupling correction of the LC-DM.

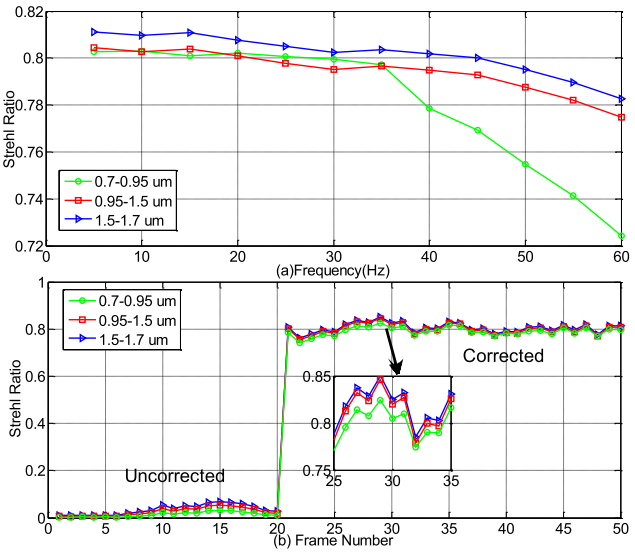

FIGURE 16. Results of the dynamic correction. (a) Relation between the frequency and SR; (b) SR values corresponding to the different wavebands, obtained after dynamic correction.

and the resolution capacity is 9.84 μm (101.6 cycles/mm). Thus, we can conclude that the diffraction-limited resolution is achieved after the global decoupling correction.

In reality, no turbulence is static. Thus, it is necessary to conduct an experiment on the dynamic turbulence correction for evaluating the practical performance of our algorithm. In our previous research, a dynamic correction could not be realized due to the complexity and time-consuming nature of the decoupling procedure. However, with the global decoupling algorithm, the WFS signal can be directly used for calculating the control signal using a one matrix calculation. This can greatly simplify the control procedure and enable the LC-DM AO to correct the aberration dynamically. In the experiment, the dynamic turbulence was generated by rotating the phase screen. The spin speed was represented the Greenwood frequency (fG) of the turbulence. The fG was varied from 10 Hz to 50 Hz, and the SR was used as the metric for quantitatively evaluating the correction results (Fig. 16(a)), and the dynamic correction procedure for 30 Hz turbulence (Fig. 16(b)).

The SR value is calculated by Equation 22, which is proportional to the residual aberration. The large stroke low spatial frequency aberration in the full waveband (0.7-1.7 um) is corrected by DM and the residual small stroke high spatial frequency aberration is corrected by LC in the visible waveband (0.7-0.95 um). Thus, the SR shows the same trend of variation but different values in separate waveband. As is well known, when SR value is greater than 0.8, the image can achieve the diffraction-limited resolution [23]. It can be seen from Fig. 16(a) that SR is greater than 0.8 when fG is

approximately 45 Hz in the 0.95-1.7 μm waveband, whereas fG is approximately 37 Hz in the 0.7-0.95 μm waveband. Hence, the DM can correct the turbulence disturbances in the infrared band around 45 Hz, and the LC-DM can correct the turbulence in the visible band around 37 Hz. Figure 16(b) shows that the SR values have reached 0.8 in different wavebands and the average SR values for the correction in the 0.7-0.95 μm, 0.95-1.5 μm and 1.5-1.7μm wavebands are 0.8014, 0.8092, and 0.8135, respectively. Thus, it can be inferred that the global decoupling algorithm can realize the diffraction-limited dynamic correction in the full waveband for the LC-DM AO system.

Based on the abovementioned experimental results, we can see that the LC-DM AO system can correct the distortions from the visible to the infrared waveband using the algorithm proposed in this study. In addition, this is the first dynamic correction of the LC-DM AO system for a 2 m telescope.

V. CONCLUSION

A global decoupling algorithm was proposed in this work. This is a simple and practical algorithm that was developed for enabling the LC-DM to simultaneously correct different spatial frequency aberrations and achieve diffraction-limited correction performance. The eigenmode orthogonal basis from the DM response matrix was derived for the DM correction. The projection of the LC response matrix onto the eigenmode orthogonal basis was derived and used for suppressing cross-coupling. Compared to the global un-decoupling algorithm and the traditional Zernike algorithm, the correction precision and cross-coupling suppression have been verified via simulation and experiments. In the simulation, the PV and RMS values after DM correction were observed to decrease from PV=2.78 μm, RMS=0.13 μm to PV=1.710 μm, RMS=0.09 μm with eigenmode and Zernike modes respectively. The coupling coefficients obtained were 0.0026 (global decoupling algorithm), 0.1893 (global un-decoupling algorithm), and 0.0108 (Zernike algorithm), respectively, which shows that the algorithm proposed in this work has the least coupling. Finally, the validity of our algorithm was experimentally proved. The atmospheric turbulence was produced using an atmospheric turbulence simulator with r0=10 cm @785 nm. The USAF target was used, and SR was used as the metric for evaluating the performance of our algorithm. After correction, USAF target images with near diffraction-limited resolution were obtained at the full waveband of 0.7–1.7 μm, which are better than those obtained using the traditional Zernike algorithm. Further, we have realized the dynamic correction of the LC-DM AO system for the first time. The experimental results indicate that 37 Hz turbulence in the visible waveband and 45 Hz turbulence in the infrared waveband can be corrected efficiently using our algorithm. This is significant from the point of view of promoting the application of the LC-DM AO system in ground-based large aperture telescopes for visible-infrared wide waveband imaging.

REFERENCES

[1] Z. Qin, S. He, C. Yang, J. S.-Y. Yung, C. Chen, C. K.-S. Leung, K. Liu, and J. Y. Qu, "Adaptive optics two-photon microscopy enables near-diffraction-limited and functional retinal imaging *in vivo*," *Light, Sci. Appl.*, vol. 9, no. 1, pp. 1–11, Dec. 2020.
[2] P. S. Salter and M. J. Booth, "Adaptive optics in laser processing," *Light, Sci. Appl.*, vol. 8, no. 1, p. 110, Dec. 2019.
[3] Y. Wang, H. Xu, D. Li, R. Wang, C. Jin, X. Yin, S. Gao, Q. Mu, L. Xuan, and Z. Cao, "Performance analysis of an adaptive optics system for free-space optics communication through atmospheric turbulence," *Sci. Rep.*, vol. 8, no. 1, p. 1124, Dec. 2018.
[4] P. Schipani, L. Noethe, D. Magrin, K. Kuijken, C. Arcidiacono, J. Argomedo, M. Capaccioli, M. Dall, S. Dorsi, J. Farinato, D. Fierro, R. Holzlohner, L. Marty, C. Molfese, F. Perrotta, R. Ragazzoni, S. Savarese, N. Rakich, and G. Umbriaco, "Active optics system of the VLT survey telescope," *Appl. Opt.*, vol. 56, no. 7, pp. 1573–1583, 2016.
[5] L. A. Poyneer, D. W. Palmer, B. Macintosh, D. Savransky, N. Sadakuni, S. Thomas, J. P. Véran, K. B. Follette, A. Z. Greenbaum, S. M. Ammons, and V. P. Bailey, "Performance of the Gemini planet imager's adaptive optics system," *Appl. Opt.*, vol. 55, no. 2, pp. 323–340, 2016.
[6] K. Matsubayashi, H. Sugai, A. Shimono, A. Akita, T. Hattori, Y. Hayano, Y. Minowa, and N. Takeyama, "Adaptive optics at optical wavelengths: Test observations of Kyoto 3DII connected to subaru telescope AO188," *Publications Astronomical Soc. Pacific*, vol. 128, no. 967, Sep. 2016, Art. no. 095003.
[7] I. D. Pater, M. H. Wong, K. D. Kleer, H. B. Hammel, M. Adamakovics, and A. Conrad, "Keck adaptive optics images of Jupiter's north polar cap and Northern Red Oval," *Icarus*, vol. 213, no. 2, pp. 559–563, 2011.
[8] K. Morzinski, B. Macintosh, D. Gavel, and D. Dillon, "Stroke saturation on a MEMS deformable mirror for woofer-tweeter adaptive optics," *Opt. Exp.*, vol. 17, pp. 5829–5844, Mar. 2009.
[9] C. Correia and J. P. Véran, "Woofer-tweeter temporal correction split in atmospheric adaptive optics," *Opt. Lett.*, vol. 37, no. 15, pp. 3132–3134, 2012.
[10] T. Cheng, Z. Xu, K. Yang, S. Wang, X. He, P. Yang, and B. Xu, "A decoupling control algorithm for Woofer–Tweeter adaptive optics system in generalized irregular pupil region," *Opt. Commun.*, vol. 472, Oct. 2020, Art. no. 125856.
[11] J. Tesch, T. Truong, R. Burruss, and S. Gibson, "On-sky demonstration of optimal control for adaptive optics at palomar observatory," *Opt. Lett.*, vol. 40, no. 7, pp. 1575–1578, 2015.
[12] T. N. Truong, A. H. Bouchez, R. S. Burruss, R. G. Dekany, S. R. Guiwits, J. E. Roberts, J. C. Shelton, and M. Troy, "Design and implementation of the PALM-3000 real-time control system," *Proc. SPIE*, vol. 8447, Sep. 2012, Art. no. 84472F.
[13] Y. K. Wang, Z. L. Cao, D. Y. Li, H. Y. Xu, and L. Xuan, "Research on the design of liquid crystal-deformable mirror adaptive optical system data acquisition and process software," *Opt. Precis. Eng.*, vol. 26, no. 6, pp. 1507–1516, 2018.
[14] H. Hofer, N. Sredar, H. Queener, C. H. Li, and J. Porter, "Wavefront sensorless adaptive optics ophthalmoscopy in the human eye," *Opt. Exp.*, vol. 19, no. 15, pp. 14160–14171, 2011.
[15] W. L. W. Liu, L. D. L. Dong, P. Y. P. Yang, A. B. X., and B. Xu, "Zonal decoupling algorithm for dual deformable mirror adaptive optics system," *Chin. Opt. Lett.*, vol. 14, no. 2, 2016, Art. no. 020101.
[16] R. Conan, C. Bradley, P. Hampton, O. Keskin, A. Hilton, and C. Blain, "Distributed modal command for a two-deformable-mirror adaptive optics system," *Appl. Opt.*, vol. 46, pp. 4329–4340, Jul. 2007.
[17] W. Zou and S. A. Burns, "Testing of Lagrange multiplier damped least-squares control algorithm for woofer-tweeter adaptive optics," *Appl. Opt.*, vol. 51, pp. 1198–1208, Mar. 2012.
[18] W. Liu, L. Dong, P. Yang, X. Lei, H. Yan, and B. Xu, "A Zernike mode decomposition decoupling control algorithm for dual deformable mirrors adaptive optics system," *Opt. Exp.*, vol. 21, pp. 23885–23895, Oct. 2013.
[19] J. F. Lavigne and J. P. Véran, "Woofer-tweeter control in an adaptive optics system using a Fourier reconstructor," *J. Opt. Soc. Amer. A, Opt. Image Sci.* vol. 25, no. 9, pp. 2271–2279, 2008.
[20] P. J. Hampton, P. Agathoklis, R. Conan, and C. Bradley, "Closed-loop control of a woofer–tweeter adaptive optics system using wavelet-based phase reconstruction," *J. Opt. Soc. Amer. A, Opt. Image Sci.*, vol. 27, no. 11, p. A145, Nov. 2010.

[21] F. Sun, Z. Cao, Y. Wang, C. Zhang, X. Zhang, Y. Liu, Q. Mu, and L. Xuan, "DM/LCWFC based adaptive optics system for large aperture telescopes imaging from visible to infrared waveband," *Opt. Exp.*, vol. 24, no. 24, p. 27494, Nov. 2016.
[22] Z. Cao, Q. Mu, H. Xu, P. Zhang, L. Yao, and L. Xuan, "Open loop liquid crystal adaptive optics systems: Progresses and results," *Proc. SPIE*, vol. 9676, Oct. 2015, Art. no. 96760E.
[23] C. Jin, X. Zhang, W. Sun, N. Li, Q. Mu, Z. Cao, Y. Wang, and L. Xuan, "Correction performance estimation of atmospheric turbulence based on eigenmode method," *Opt. Commun.*, vol. 466, Jul. 2020, Art. no. 125661.
[24] R. J. Noll, "Zernike polynomials and atmospheric turbulence," *J. Opt. Soc. Amer.*, vol. 66, no. 3, pp. 207–211, 1976.
[25] X. Zhang, Z. Cao, C. Yang, Z. Peng, Q. Mu, and L. Xuan, "Improved bandwidth of open loop liquid crystal adaptive optics systems with a proportional-derivative controller," *Opt. Exp.*, vol. 27, no. 8, Art. no. 11651, Apr. 2019.
[26] J. G. Ziegler and N. B. Nichols, "Optimum settings for automatic controllers," *J. Dyn. Syst., Meas., Control*, vol. 115, no. 2B, pp. 220–222, Jun. 1993.
[27] X. Zhang, Z. Cao, Q. Mu, D. Li, Z. Peng, C. Yang, Y. Liu, and L. Xuan, "Progress of liquid crystal adaptive optics for applications in ground-based telescopes," *Monthly Notices Roy. Astronomical Soc.*, vol. 494, no. 3, pp. 3536–3540, May 2020.

YUKUN WANG was born in 1988. He received the B.S. and M.S. degrees in control science and engineering from Beihang University, in 2010 and 2013, respectively, and the Ph.D. degree in optical engineering from the University of Chinese Academy of Sciences, Beijing, China, in 2019. From 2013 to 2021, he was a Research Assistant with the State Key Laboratory of Applied Optics, Changchun Institute of Optics, Fine Mechanics and Physics, Chinese Academy of Sciences. His research interests include adaptive optics control systems and its application.

XINGYUN ZHANG was born in 1988. He received the B.S. degree in automation from the University of Science and Technology of China, Hefei, China, in 2010, and the M.S. and Ph.D. degrees in optical engineering from the University of Chinese Academy of Sciences, Beijing, China, in 2015. From 2015 to 2021, he was an Associate Researcher with the State Key Laboratory of Applied Optics, Changchun Institute of Optics, Fine Mechanics and Physics, Chinese Academy of Sciences. His research interests include the development of adaptive optics and its application.

DAYU LI was born in 1979. He received the Ph.D. degree in optical engineering from the University of Chinese Academy of Sciences, Beijing, China, in 2007. From 2007 to 2009, he was a Research Assistant with the State Key Laboratory of Applied Optics, Changchun Institute of Optics, Fine Mechanics and Physics, Chinese Academy of Sciences, where he was an Associate Researcher, from 2019 to 2021. His research interests include wavefront reconstruction and image processing with GPU.

QUANQUAN MU was born in 1980. He received the B.S. degree in physics from Nankai University, Tianjin, China, in 2003, and the M.S. and Ph.D. degrees in optics from the University of Chinese Academy of Sciences, Beijing, China, in 2010. Currently, he is a Professor and the Deputy Director with the State Key Laboratory of Applied Optics. His research interest includes the design of the adaptive optics systems.

LI XUAN was born in 1957. She received the B.S. degree from Jilin University, in 1983, the M.S. degree from the Changchun Institute of Physics, Chinese Academy of Sciences, in 1986, and the Ph.D. degree in engineering from Tohoku University, Japan, in 1998. She was selected into the Chinese Academy of Sciences/Hundred Talents Program, in 1999. Her research interests include liquid crystal adaptive optics, liquid crystal research on optical devices, and liquid crystal polymer chemistry.